Chapter 7

Impact of 13-93 bioactive glass addition on the machinability behavior of 3Y-TZP-based biocomposite materials

7.1 Introduction

Nowadays, bio-ceramic composite material is in demand in the biomedical industry due to its remarkable biological and mechanical properties. But, the shaping of such material challenges the manufacturer. Ceramic materials containing 3 mol% yttria-stabilized zirconia (3Y-TZP) have been used in biomedical applications for a long time (Piconi *et al.*, 1999). Because of these materials' excellent mechanical strength and biocompatibility, they have several uses in the disciplines of orthopedics and dentistry. Similarly, bioactive glasses have been also used in biomedical industries due to their excellent biological properties (Yadav *et al.*, 2020). Researchers reported that 3Y-TZP-based BG bioceramic composites have wide applications in the biomedical field as implant components because the addition of BG into 3Y-TZP enhances the biological properties of 3Y-TZP (Ho *et al.*, 2011) (Habibe *et al.*, 2009) (de Paula *et al.*, 2019). Before implantation, the implant needs to be processed into a particular shape and size with patient geometry for its proper function in the human body because the geometry of the implant may vary from person to person. So, it is essential to explore the machining studies of bioceramic composite materials. Some researchers have studied the machinability of bioceramic composite materials in terms of drillability, cutting, grinding, and MRM by different conventional machining techniques and also checked the effects of different process parameters on their machinability (Amat *et al.*, 2019) (Li *et al.*, 2021) (Ghosh *et al.*, 2016).

However, many researchers have reported conventional machining of bioceramic materials and found it to be the biggest challenge in manufacturing due to its inherent high brittleness and hardness nature (Ghosh *et al.*, 2016). Conventional machining exhibits many limitations, such as the high cost of tools, more time-consuming, low surface finish, and difficulty in making

complex geometry (Mehta *et al.*, 2021) (Jain, 2009). These problems have drawn the attention of researchers worldwide to switch towards unconventional techniques of machining.

Air abrasive jet machining (AAJM) is one of the most alluring unconventional machining techniques for degrading non-conductive materials with hard surfaces and brittle materials (Diaz *et al.*, 2019) (Rayat *et al.*, 2017). It has less thermal and mechanical residual stresses generated during machining. The other benefits are high MRR, a cheap manufacturing cost, and ease of setup (Melentiev *et al.*, 2018) (Dehghanghadikolaei *et al.*, 2018). In AAJM, the basic concept of machining is mechanical erosion by abrasive particles, and the machinability is assessed in terms of MRR and SR (Rayat *et al.*, 2017). Material characteristics, including hardness, toughness, and elastic modulus, have an impact on the MRR and SR (Evans *et al.*, 1978) (Wiederhorn *et al.*, 1979) (Ritter *et al.*, 1984). Researchers have also found that the striking angle, temperature, and types of abrasive materials significantly affect the machinability. Further, it is noticed that the MRR of brittle material is the maximum at 90° striking angle and increases with increasing machining temperature (Bhushan, 2001) (El-Domiaty *et al.*, 2009) (Fang *et al.*, 2015).

Few authors have reported the machining of 3Y-TZP ceramics by the AAJM method and evaluated the effect of different process parameters on MRR (material removal rate), SR (surface roughness), and MRM (material removal mechanics) (Fang *et al.*, 2015) (Fang *et al.*, 2015) (Zhao *et al.*, 2022). It is concluded that machining temperature, striking angle, and material properties have significantly affected the MRR, SR, and MRM. The materials are removed from the sample surface by an erosion crater accompanied by exfoliation at room temperature while at high temperature due to plastic deformation with ploughing. Some researchers have also studied the machining performance of BG with AAJM (Park *et al.*, 2004) (Jagannatha *et al.*, 2012) (Abdelnasser *et al.*, 2016). The machinability is strongly affected by the different variables such

as striking angle, types of abrasive, and machining temperature. It is also observed that the material is removed from the workpiece in a brittle manner with grain ejections.

In the present work, the main objective is to study the machinability behavior of 3Y-TZP/13-93 BG composite materials in terms of MRR and SR at ambient and elevated temperatures and make them useful for biomedical applications as dental materials. Bioceramic composite materials, having general weight composition [(100-x) (3Y-TZP) – x (13-93 BG)] where x = 0 to 25 wt%, have been prepared. Sample identification and different compositions of biocomposite materials are given in Table 3.1 and their machinability in terms of MRR, SR, and MRM is studied as a function of BG composition and machining temperature.

7.2 Results and discussion

7.2.1 Abrasive air jet machining at room and elevated temperature

7.2.1.1 Abrasive materials and surface morphology before machining

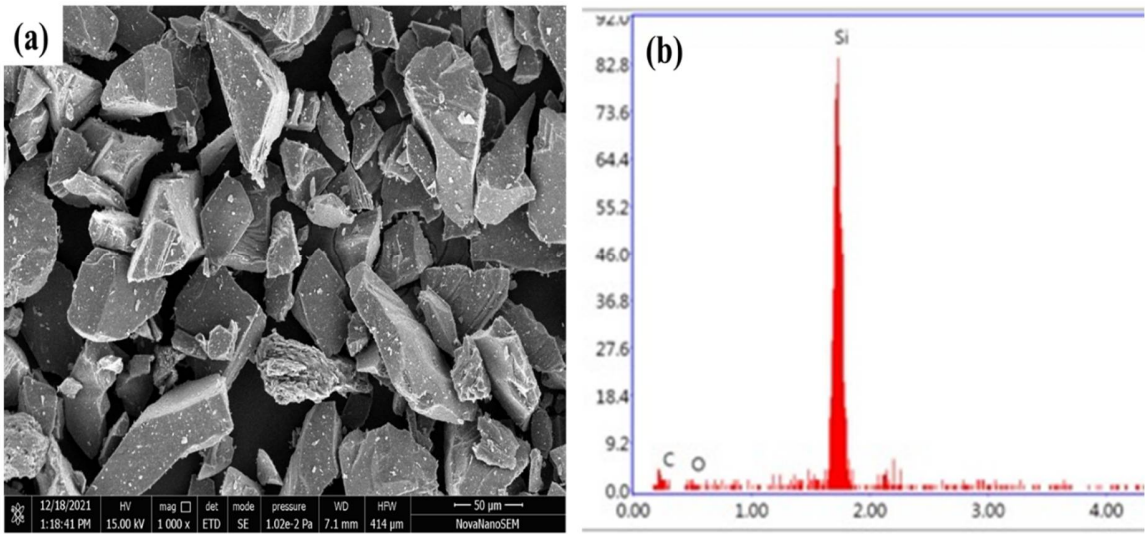

Fig.7.1 (a) HR-SEM image and (b) elemental analysis of erodent (SiC) material.

The particle shape of erodent SiC was seen with HR-SEM and represented in Fig. 7.1(a). EDS image (Fig. 7.1(b)) of the abrasive materials confirms the presence of Si and C elements. No other impurities are present in the powder. Before machining, the HR-SEM and EDS images of ZBG0 (Pure) and ZBG25 are shown in Fig. 7.2.

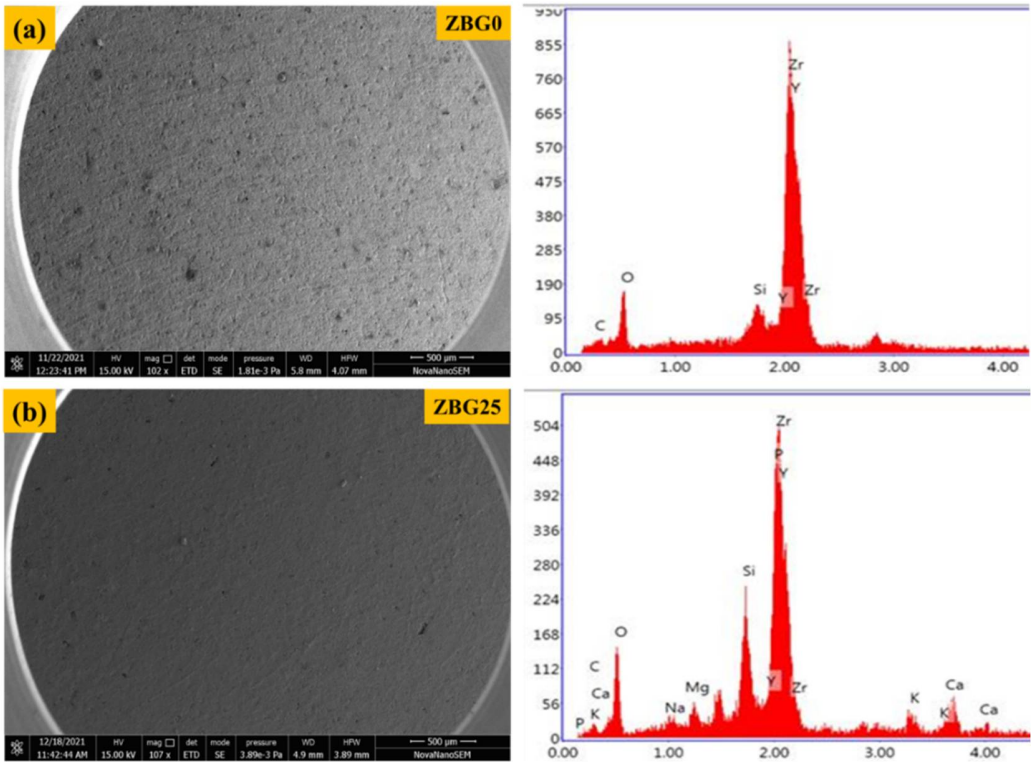

Fig. 7.2 HR-SEM and EDS images of (a) x = 0, (b) x = 25 wt% sintered [(100-x)(3Y-TZP) - x(13-93 BG)] composites at room temperature.

7.2.1.2 Effect of BG additions on the MRR

Fig. 7.3 shows the MRR of ZBG0 and composites samples as the function of BG contents at room and elevated temperature under normal jet striking conditions. Notably, the MRR of this composite material is remarkably decreased in both conditions, at the room, as well as elevated

temperature with BG contents. With increasing the BG content, the MRR of composite materials continuously decreases up to 25 wt%, as the hardness significantly affects the erosion resistance of ceramic materials (Hang *et al.*, 2016) (Srinivasan *et al.*, 1988) (Wellman *et al.*, 1995). Also, deformation occurs easily when compressive stress is applied to materials with low mechanical strength and hardness. It is a favorable condition for stress dissipation rather than developing new surfaces by crack initiation and propagation. It is noticed that the addition of 13-93 BG into 3Y-TZP ceramic effectively increases the hardness and imparts the 3Y-TZP/13-93BG composite with improved erosion resistance against MRR at the room and elevated temperatures.

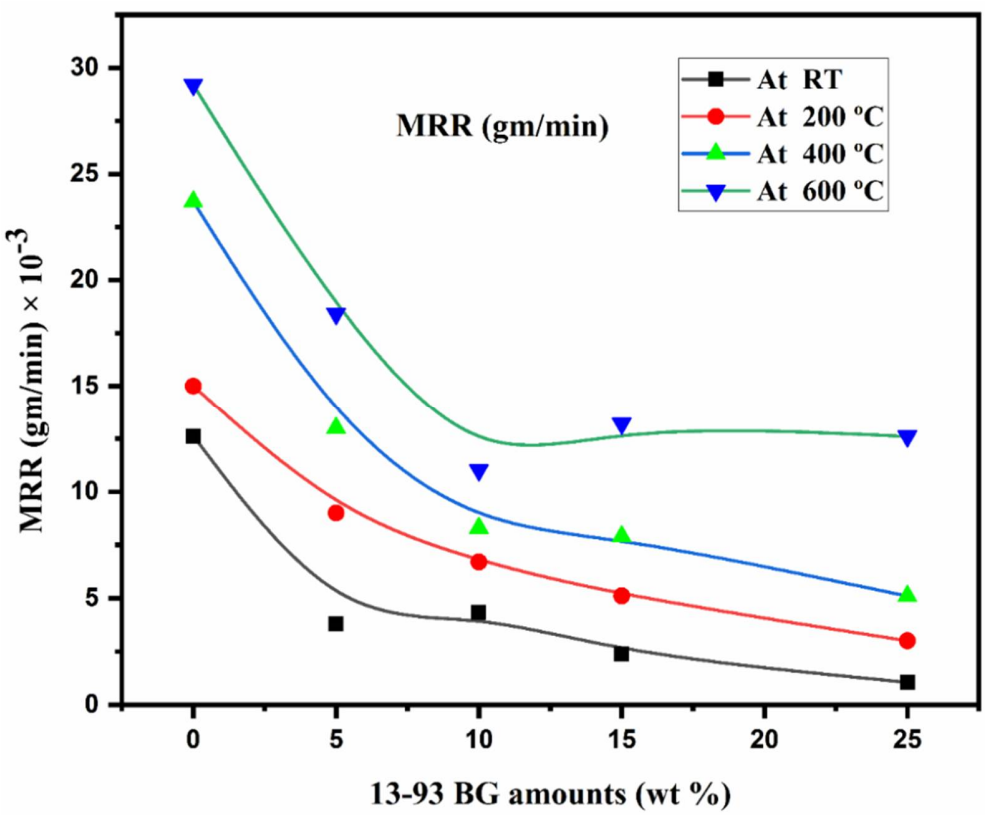

Fig. 7.3 MRR of composite materials as a function of BG content and machining temperatures.

Besides the hardness, the microstructure may beneficially change due to the addition of BG, which may also be accountable for the better erosion resistance of the 3Y-TZP/13-93BG

composite materials (Hang *et al.*, 2016). As shown in Fig. 4.3(a-h), the grain size of the composite materials is decreased with increasing the BG addition into pure 3Y-TZP ceramic. Due to decreased grain size, interspaces between the particles are increased. Generally, compared to the less porous material, the more porous material is more susceptible to MRR (Abdelnasser *et al.*, 2016). However, in this experiment, the MRR is decreased with increasing the porosity. The reasons for less MRR are due to the interspaces and porosity present due to low sintering temperatures. It is filled by infiltration of the semi-liquid glass due to lowering the viscosity of the BG, as shown in Fig. 4.3(b, d, f, and h). This infiltrated BG is wetted the matrix particle and combined with these particles. The grains are not easily ejected from the surface of composite materials. Besides wetting the matrix surfaces, the semi-liquid BG also fills the interspaces between the grains, as shown in Fig. 4.3(d and f), and creates a hindrance for the particles to be ejected. So, the infiltration of BG may enable the removal of pores and reduce the unwanted gathering of glassy phase in the composite, as shown in Fig. 4.3(d, f, and h), which makes the more erosive resistant to composite samples. The particles are not easily eroded from the samples. Consequentially, MRR decreases with increasing the BG addition.

7.2.1.3 Effect of machining temperature on the MRR

The MRR of ZBG0 and composite materials as a function of machining temperature are represented in Fig. 7.3. The MRR of pure 3Y-TZP and the composite materials are increased with increasing the machining temperature. At room temperature (RT) and 600^{o}C, the MRR of pure 3Y-TZP is 12.62 $\times 10^{-3}$ and 29.20 $\times 10^{-3}$ gm/min, respectively. It is significantly greater than ZBG5, ZBG10, ZBG15, and ZBG25 composite material samples. The MRR of composite materials is also increased with increasing temperature. The difference in MRR is caused by the

deterioration of the mechanical properties of composite materials at elevated temperatures (Hang *et al.*, 2016); consequently, there is a change in the MRM (Munro, 2005). Another reason may be due to increasing the size of radial cracks, which is initiated during the striking jet of abrasive, as the temperature of composite samples is increased. This radial fissure promotes erosion and chip-like material loss from the samples due to erosion (Jagannatha *et al.*, 2012). Generally, crack initiation occurs in a brittle manner at low temperatures. Further, deep chip formation takes place by plastic deformation with increasing temperature. As a result, the MRR rises, indicating that temperature has a significant impact on the MRR (Hang *et al.*, 2016) (Jagannatha *et al.*, 2012) (Hang *et al.*, 2016).

7.2.1.4 Machined surface morphology at room temperature

The machining of the ZBG0 sample is represented in Fig. 7.4(a, b), representing a very rough surface and random erosion. The eroded surface has some deep erosion craters and some shallow erosion craters accompanied by exfoliation, cracks, and brittle fractures after the impact of hard erodent particles. The eroded surface morphology of the ZBG10 sample is represented in Fig. 7.4(c, d), which shows that materials are not easily eroded. This erosion takes place mainly by the erosion crater. There are many small erosion craters, and some porosity is also present on the machined surface. It is found that due to the inclusion of 10 wt% of BG, the sample becomes dense with improved mechanical strength and hardness, which leads to a decrease in MRR as compared to the previous sample. Further, the MRR is decreased with BG addition up to 25 wt%, and the porosity is increased, as represented in Fig. 7.4(e to h). The morphology of the samples indicates that the erosion occurs due to a large erosion crater accompanied by exfoliation.

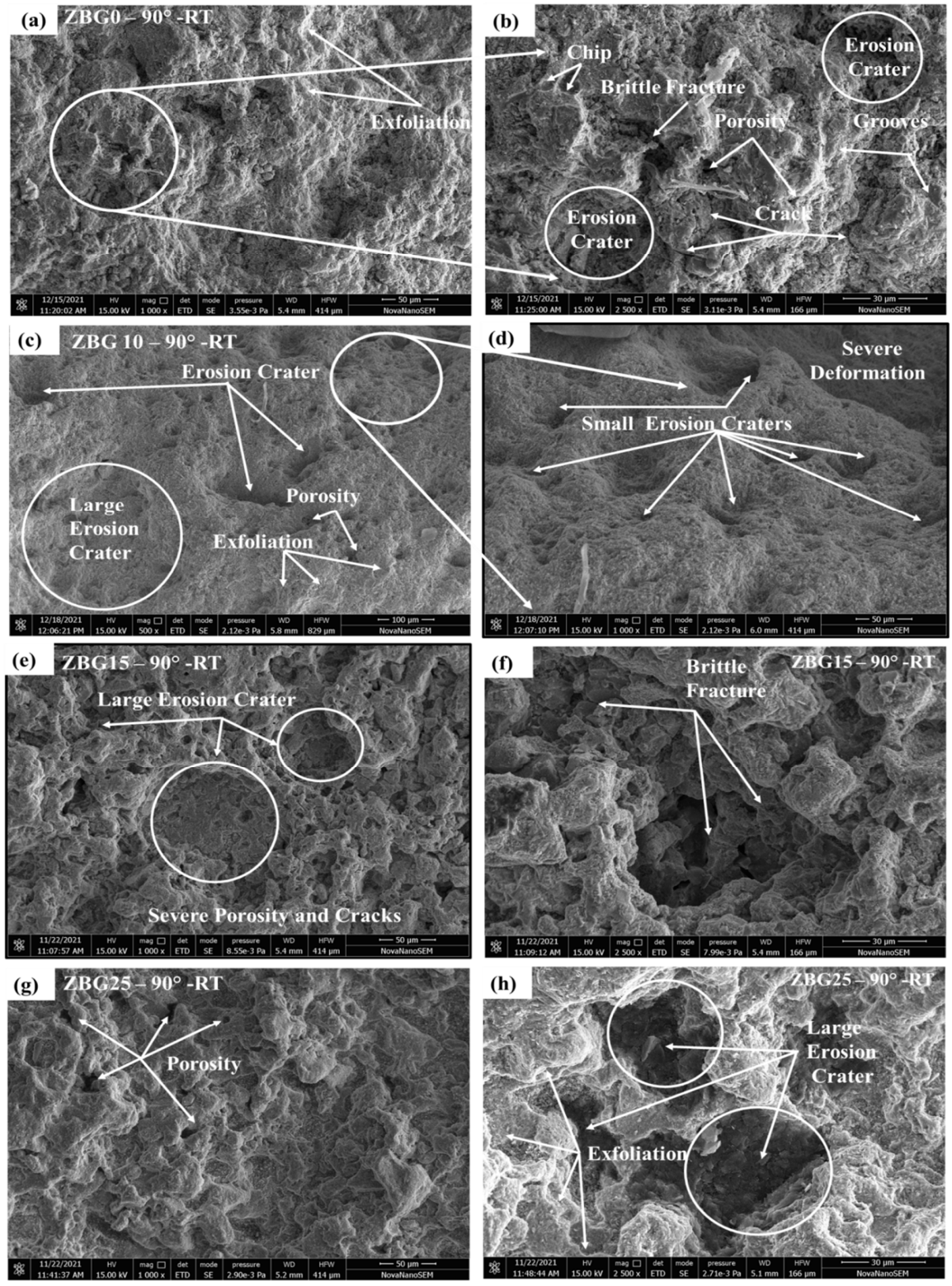

Fig. 7.4 HR-SEM of the machined surface at room temperature.

7.2.1.5 Machined surface morphology at elevated temperature

At high-temperature machining, the machining behavior of the pure 3Y-TZP (ZBG0) sample (Fig. 7.5(a)) shows similarity with the room temperature morphology.

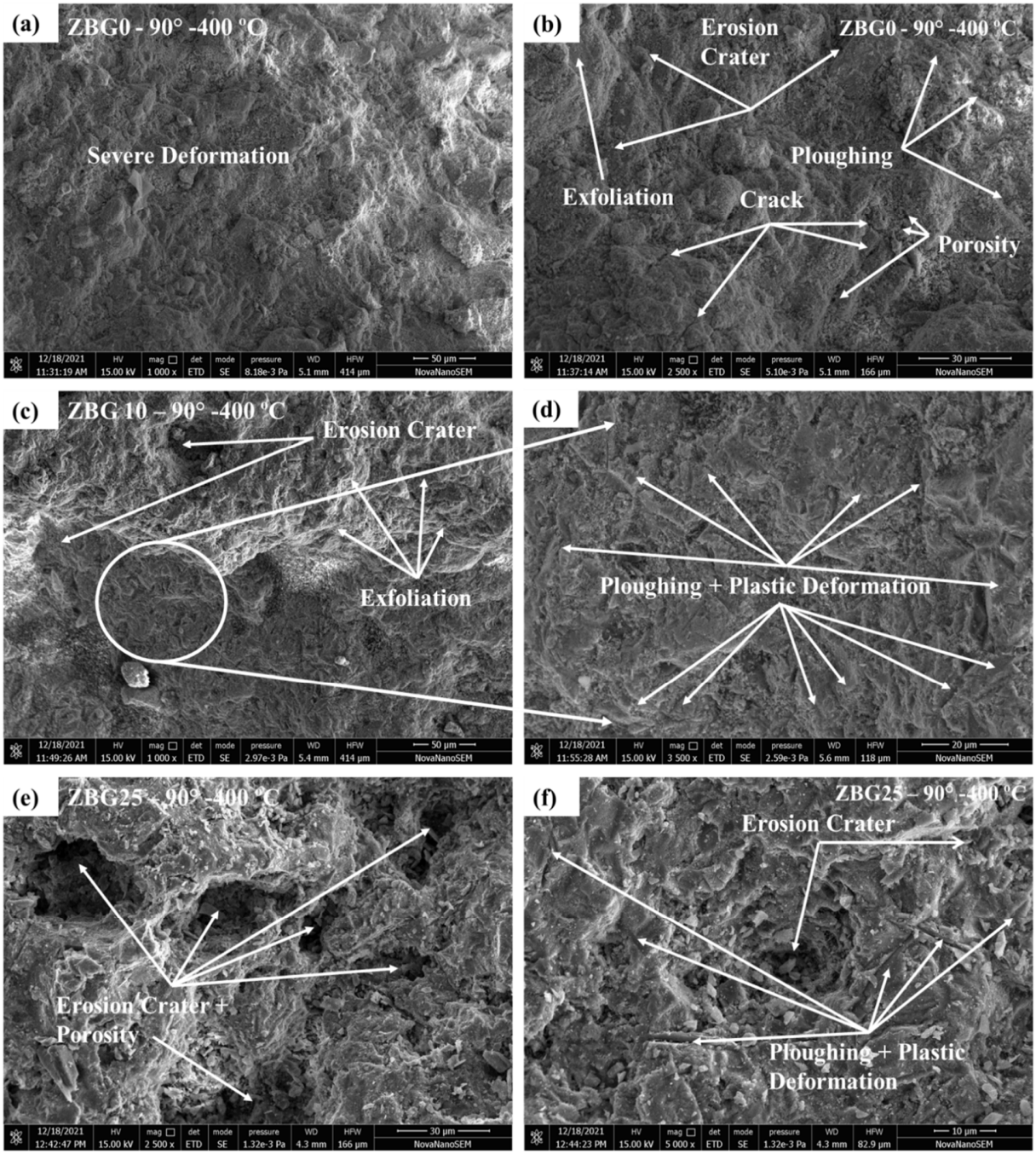

Fig. 7.5 HR-SEM of the machined surface at 400ºC temperature.

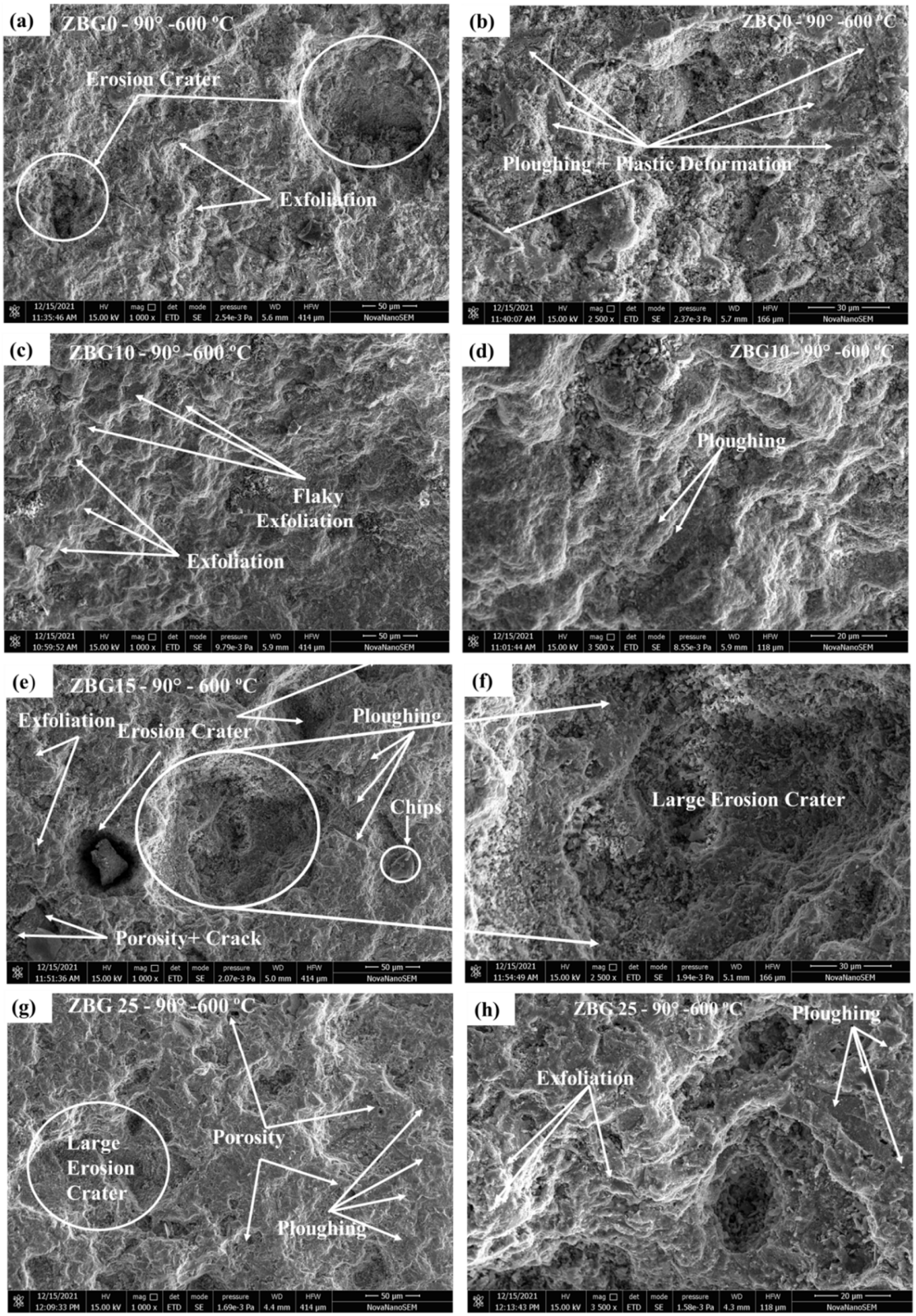

Fig. 7.6 HR-SEM of the machined surface at 600ºC temperature.

When the machining temperature is raised from room temperature to 400ºC, the material is eroded by ploughing, which is accompanied by erosion craters, as represented in Fig. 7.5(b). It shows that plastic deformation begins at this temperature. The machined surface of the ZBG10 sample (Fig. 7.5(c & d)) represents some visible grooves that are generated by the sliding motion of hard abrasive particles, and the material is removed by plowing action accompanied by plastic deformation. In the ZBG25, the materials are eroded by the large-size erosion craters and ploughing, as observed in Fig. 7.5(e, f). Similarly, when the machining temperature is increased up to 600ºC, the erosion takes place in the ZBG0 sample by the erosion crater (Fig. 7.6(a)) with a large width, along with plastic deformation and ploughing (Fig. 7.6(b)), which occurs by sliding of impacted hard erodent particles. When BG concentration is increased, the material removal occurs by the large size of multiple erosion craters along with ploughing, as shown in Fig. 7.6(c, d, e, f, g, h). The erodent-surface interactions create firm wear debris, which is highly damaged and piled up at the grooves' corners.

7.2.1.6 The machined surface topographies

The machined surface topographies of the 3Y-TZP and BG-based composites are shown in Fig. 7.7 and Fig. 7.8 in three-dimensional (3D) form. It shows the machining wear and SR both in the room and at elevated temperatures. The machining temperature is varied from room temperature to 600ºC, and other process parameters are kept constant. Some peaks and valleys exist on the machined area of the composite materials. The prominent peaks and valleys indicate the mass of troughs, pits, and residual bulges generated during materials removal. The topography structures that are depicted match up properly with the HR-SEM images of the

machined samples. Fig. 7.9 shows the bar chart of SR variation with increasing BG amounts and the machining temperature.

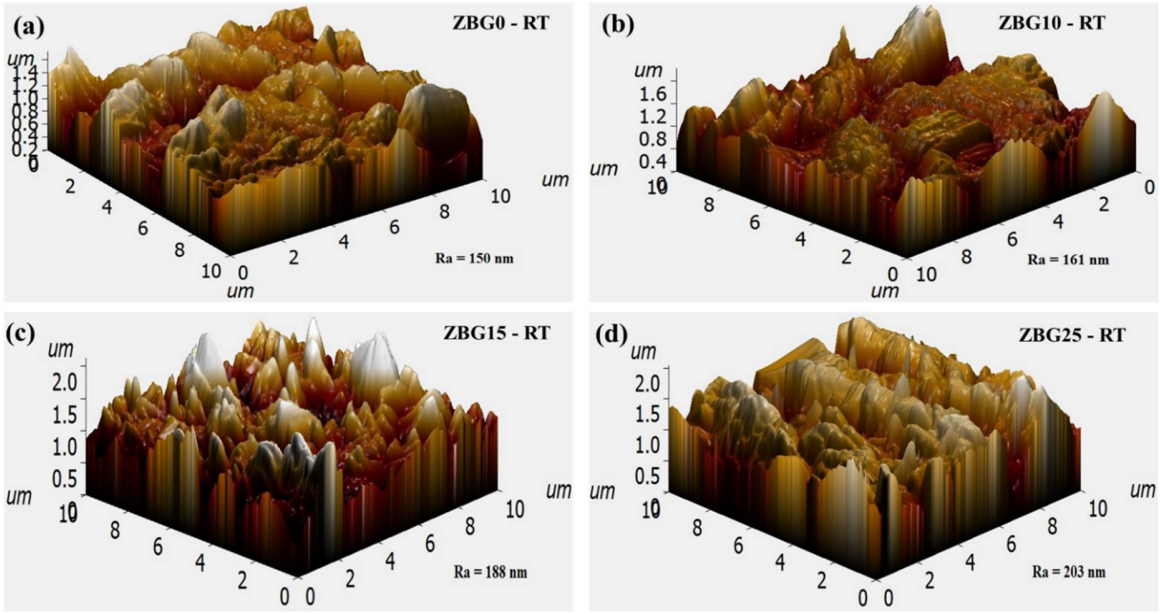

Fig. 7.7 Topography of the machined surface at room temperature.

At room temperature, the obtained SR values of ZBG0, ZBG10, and ZBG25 are 150±10, 161±9, and 203±12, respectively. The SR increases with increasing the BG content into 3Y-TZP ceramic, as shown in Fig. 7.9. Also, it is observed that a better surface finish is detected in the samples that contain less BG content. A better surface finish indicated that the matrix and reinforcement particles may be simultaneously eroded from the workpiece surface. It may be due to more surfaces of hard particles (3Y-TZP) available for erosion. With increasing the BG content into 3Y-TZP ceramic, more grains of BG may be available on the surface of the workpiece. Since the hardness of BG is less in comparison to 3Y-TZP at room temperature (de Paula *et al.*, 2019) (Jagannatha *et al.*, 2012) and the particle size of BG is larger than pure 3Y-

TZP ceramic, it may be a possibility that the BG grain may be detached from the workpiece surface easily.

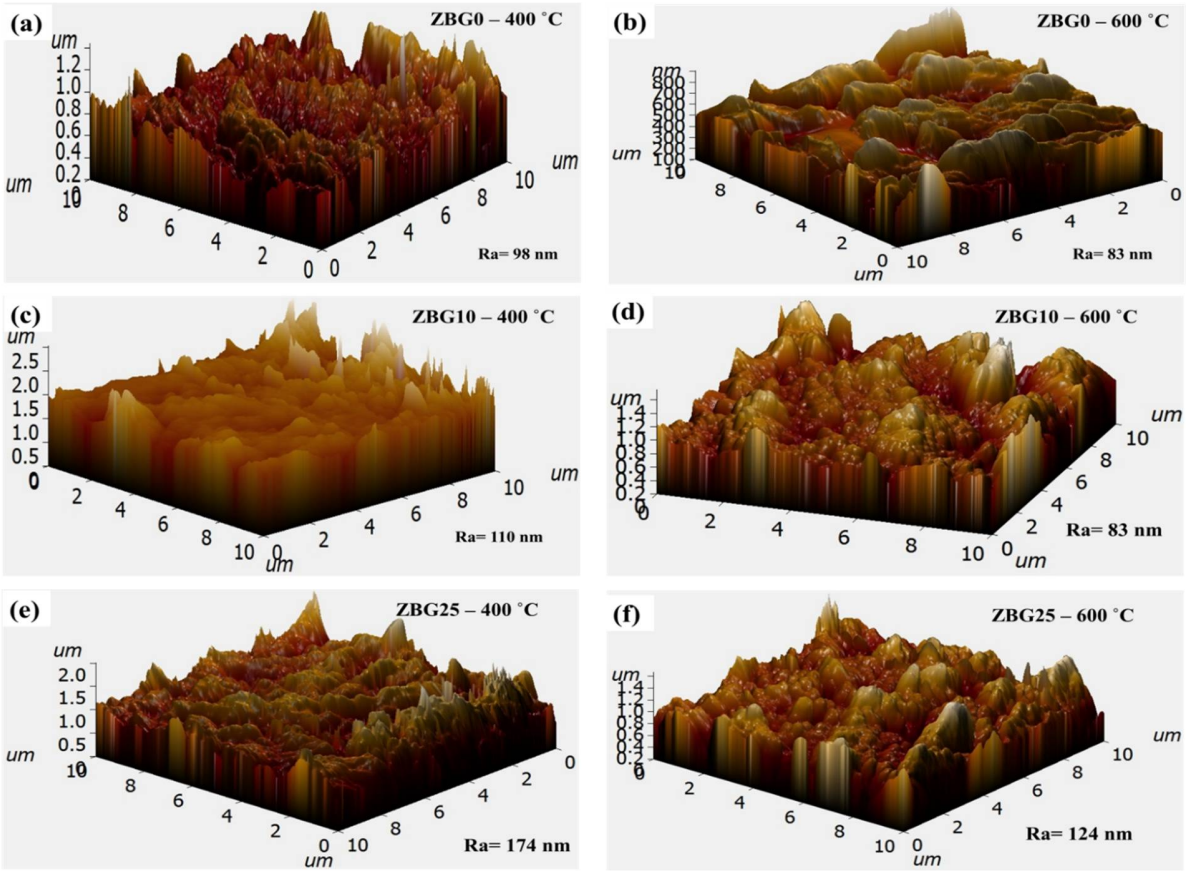

Fig. 7.8 Topography of the machined surface at elevated temperatures.

Some pits and erosion craters (Fig. 7.4) may be generated on the machined surface; hence, high SR is observed at a high content of BG. Matías F. Stábile *et al.* have studied the effect of BG addition on different characteristics of Y-TZP ceramic and reported that SR of Y-TZP ceramic increases with increasing the BG amount addition into Y-TZP (Stábile *et al.*, 2019). At the microstructure level, the formation of the m-ZrO_2 phase can be attributed to the undesirable martensitic transformation during the cooling of the sintered samples (Ho *et al.*, 2011) (Habibe *et al.*, 2009) (de Paula *et al.*, 2019). The formation of the m-ZrO_2 phase is increased with the

addition of BG contents, as observed in Table 4.1 of Chapter 4. This martensitic transformation promotes a volumetric expansion, which leads to micro-cracking and an increase in the formation of porosity in sintered samples during cooling (Habibe *et al.*, 2009). The surface roughness of the machined surface is strongly affected by surface properties and the porosity present in the samples (Jain, 2009) (Abdelnasser *et al.*, 2016). The cracks and porosity present in the samples destroy the surface finish of the machined surface and hence increase the surface roughness, as shown in Fig. 7.9. In addition to this, the infiltration of BG into 3Y-TZP wets the matrix particle and combines with these particles, as shown in Fig. 4.3(b, d, f, and h) of Chapter 4; due to this these grains are ejected in the form of large and irregular shape particles, which destroy the surface finish of the machined surface of composite materials. It can be clearly observed by SEM image in Fig. 7.4(f, and h).

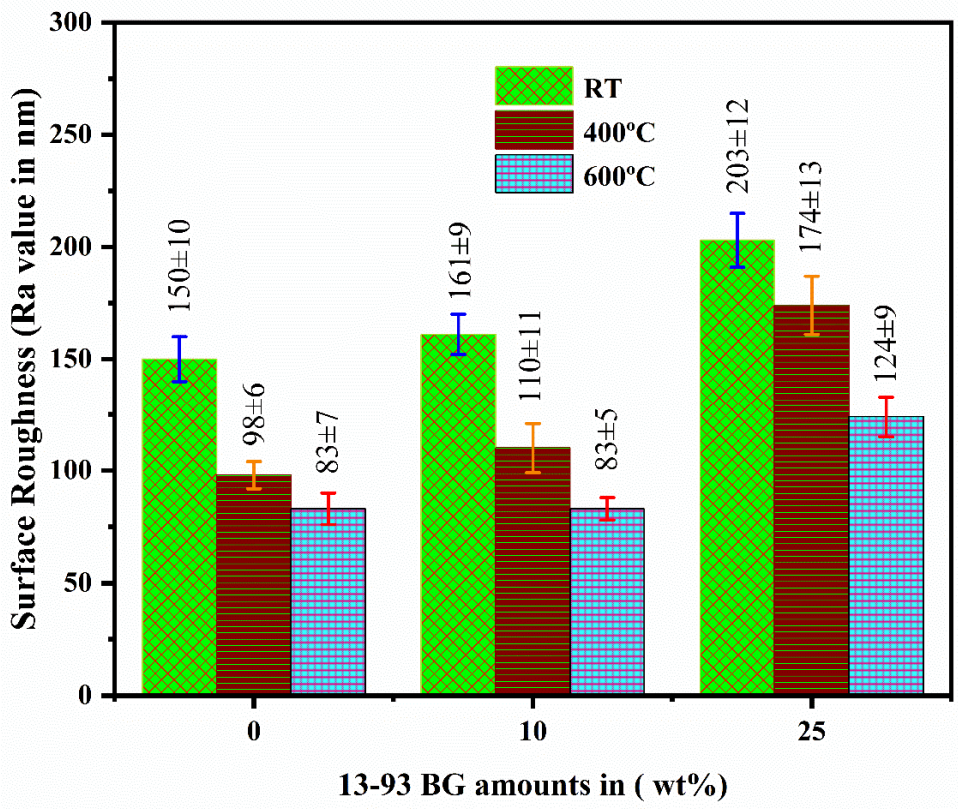

Fig. 7.9 Surface roughness (nm) of the machined surface at room and elevated temperatures.

From Fig. 7.9, the obtained SR values of ZBG0, ZBG10, and ZBG25 are 98±6, 110±11, and 174±13 at 400ºC and at 600ºC 83±7, 83±5, and 124±9, respectively. At higher temperatures, the SR value is decreased by increasing the machining temperature up to 600ºC. When the machining temperature is increased from room temperature, more materials are removed by the plastic deformation accompanied by plowing action, which helps in forming larger and wider chips from the workpiece surface. The eroded materials in the form of chips and larger fractures result in a new smooth bottom of the sample, reducing the SR of the samples. The created new bottom surface is more flexible, increasing the smoothness of the surface (Fang *et al.*, 2015).

7.2.1.7 Material removal mechanics

The machining behavior of ceramic composite materials can be clearly understood by the elastic-plastic model given by Marshall, Lawn, and Evans (Evans *et al.*, 1978) (Wiederhorn *et al.*, 1979) (Marshall *et al.*, 1982), established on the assumption of lateral fracture. It is well known that ceramic materials behave differently due to crystal structures and erosion processes. In some cases, the wear mechanism cannot be well explained. According to numerous experts, ceramic materials are eroded not only by brittle fractures but also through ductile and brittle fractures (Alman *et al.*, 1999) (Fang *et al.*, 1999) (Oka *et al.*, 2009). The improvement in the mechanical characteristics of the present composite samples leads to a change in the mechanism of material removals (Tang *et al.*, 2016). In this work, it is observed that 3Y-TZP/13-93 BG composites show different erosive resistant natures and machined surface morphologies, studied under various conditions like the inclusion of 13-93 BG concentration at room and elevated temperature. It can be explained on the basis of Evans's elastic-plastic models and the ductile-brittle transition model during machining (Evans *et al.*, 1978) (Wensink *et al.*, 2002). According

to Evans's elastic-plastic model, plastic deformation is produced on the impacted area when hard and rigid abrasive particles strike the ceramic material surface. The affected surface of the biocomposite samples absorbs the kinetic energy of the impacting erodent's particles. At that instant, tensile stress is increased in the deformed area, leading to crack initiation and propagation. The ductile-brittle transition model describes that the materials are eroded from the ceramic surface by cutting and ploughing. This brittle and ductile erosion can be clearly seen in HR-SEM images in Fig. 7.4(f) and Fig. 7.5(d).

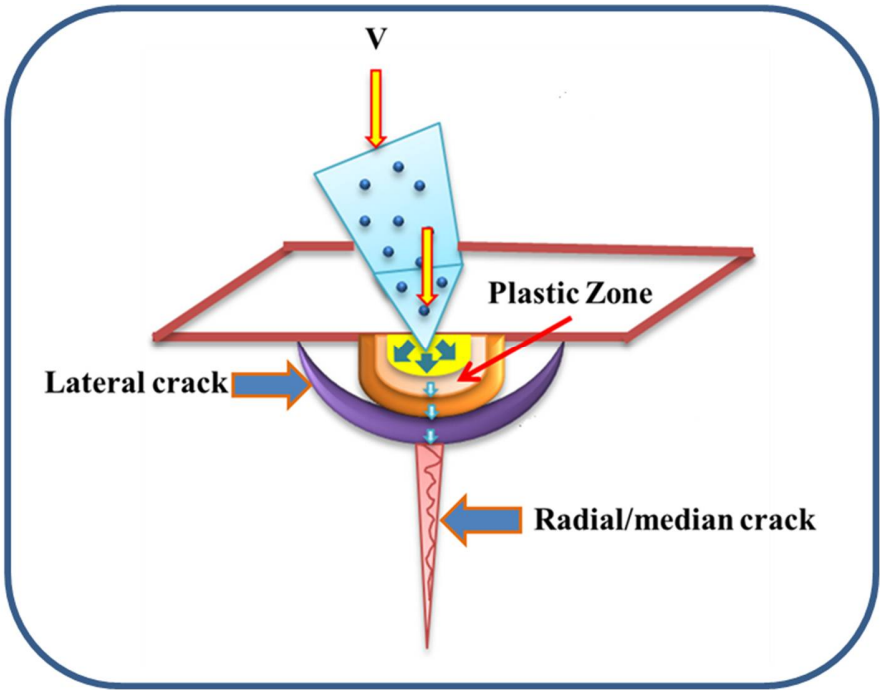

Fig. 7.10 The schematic diagram of lateral and radial crack formation and propagation

According to the previously reported machining model (Jain, 2009), due to the compressive force, a plastic deformation zone was formed beneath a sharp indenter tip as it penetrated into the interior of the workpiece. As the compressive force increased, the created plastic zone was expanded. The radial/median and lateral cracks eventually developed along the

surface's perpendicular as well as parallel directions, respectively, as shown in Fig. 7.10. At this moment, it might be considered that the radial/median cracks were related to the creation of surface cracks, whereas the lateral fractures were related to the workpiece removal procedure in AAJM. As the depth of the machined material increased, it was crucial in various ways to expedite the removal process.

Another well-established model exists to explain the erosion of brittle materials like ceramics (Shipway *et al.*, 1996). In this model, it is reported that the ratio of SiC hardness (Hs) to the hardness of the composite material (Hc) has a strong effect on erosion mechanics. When Hs/Hc > 1, the material removal occurs by the large erosion crater, plastic deformation, and plowing action. The erosion crater may be radial or lateral. The radial cracks grow and propagate in the direction of impact, whereas lateral cracks grow and extend from the attacked point parallel to the sample surface. When Hs/Hc < 1, the erodent materials are not capable of eroding the material from the target samples, and it is very tough to grow and propagate radial and lateral cracks in the sample, leading to a significant decrease in MRR.

As the machining temperature increases, particularly above 200ºC, the mechanical properties may be severely reduced due to bond strength degradation at high temperatures (Jagannatha *et al.*, 2012) (Tang *et al.*, 2016) If the target material is softer than the erodent material, the rate of strain is decreased, hard abrasive particles slide over the composite surface, and the target materials are cut by plowing. It leads to the production of extended plastic grooves on the targeted surfaces, as represented in Fig. 7.5(d, f). In the previous research, it is stated that above the glass transition temperature (Tg), the glass phase has a tendency to exhibit a viscous behavior, leading to some plasticity (Nawaz *et al.*, 2021), which may also be a cause of plastic deformation and materials removal by ploughing at elevated temperature. In the experiment, the

mass flow rate of erodent particles and machining velocity are taken constantly. A constant momentum jet of harder particles is formed, which strikes the sample surface and produces severe damage, as shown in Fig. 7.6(f). Therefore, at high-temperature machining, erosion occurs mainly by plowing action accompanied by subsurface micro-cracks, primarily responsible for dispersing the striking energy of abrasive particles. The plastic deformation also takes place in monolithic 3Y-TZP ceramics at elevated temperatures due to their microstructural changes and decreased mechanical properties (Fang *et al.*, 2015).

7.3 Summary

In the present investigation, the [(100-x) (3Y-TZP) – x (13-93 BG)] bioceramic composite materials are synthesized and checked the machinability behavior in the form of MRR, SR, and MRM of these materials. The 3Y-TZP ceramic composite with 10 wt% of BG content is found to be machinable with better mechanical properties. The content of BG and machining temperature are observed as significant parameters for both MRR as well as SR. The SR of the machined surface is observed as an increasing trend in increasing the additions of BG content. At the same time, it follows a decreasing trend of increasing the machining temperature. Analysis of machined surface indicates that mainly ploughing with plastic deformation and large erosion craters are the predominant mechanisms at an elevated temperature. While at room temperature, brittle fracture, grain ejection, micro-crack propagation, and exfoliation are responsible for material removal. A comparison between previously reported research work and the present research study on the machining of bioceramic materials/composites is summarised in Table 7.1.

Table 7.1 Comparison of previously reported research works on machining of bioceramic/ceramic-based composite materials with present machined materials.

S. No	Materials	Application	Machining technique	Machining performances	Remarks
1.	ZrO_2 Block (Amat *et al.*, 2020)	Biomedical applications	Conventional CAD/CAM milling	Cutting grooves	Machinability depends on presintering temperature
2.	HA-$LaPO_4$ Biocomposite (Ghosh *et al.*, 2016)	Biomedical applications	Conventional radial drilling machine	Drillability, thrust force, and torque	Machinability increased with contents of $LaPO_4$ enhancement
3.	3Y-TZP Ceramic (Fang *et al.*, 2015)	High-temperature application	Abrasive air jet machining	MRR	MRR increased with experimental temperature, maximum MRR at 1200^oC
4.	Soda Lime Glass (Jagannatha *et al.*, 2012)	Industries and laboratory	Abrasive air jet machining	MRR, SR	MRR 1.4 to 1.7 times greater, and SR reduced by 4-10% at a higher temperature of 310^oC
5.	$LaMgAl_{11}O_{19}$-Al_2O_3 (Srinivasan *et al.*, 1988)	Industries	Abrasive air jet machining	MRR, SR, MRM	Significant effect of temperature, angle, and abrasive particles on MRR. SR 24.24% increased with

					machining temperature 1200°C at 60°
6.	Glass and GFRP (Suresh *et al.*, 2018)	Industries and laboratory	Abrasive air jet machining	MRR	MRR increased with jet pressure, maximum MRR at 6 bar
7.	Y-TZP Ceramic (Kim *et al.*, 2002)	High-temperature application	Abrasive air jet machining	MRR	MRR increased with machining temperature with a velocity up to 70 m/sec.
8.	Human Dentin (Kohorst *et al.*, 2014)	Biomedical applications	Abrasive water jet machining	MRR and drilling depth	significantly increased by abrasive and pressure of water (15 to 25 MPa)
9.	Bovine Bone (Wei *et al.*, 2021)	Biomedical applications	Conventional self-centering drill bit	Drillability	Less temperature generated, and machinability improved
10.	(Ce, Y)-TZP/Al_2O_3 (Alves *et al.*, 2022)	Dental applications	Grinding with 15 and 45 μm sandpaper	Effect of SR on biological /mechanical properties	The best cellular attachment and proliferation are shown in the rougher materials, with slightly reduced mechanical qualities.
11.	3Y-TZP (Ji *et al.*, 2021)	Biomedical applications	Milling Machining	Sintering temperature and	Due to their usual ductile-brittle removal properties, the 1200°C sintered ceramic

				machinability	samples exhibit the best machinability.
12.	3Y-TZP (Amarante *et al.*, 2019)	Dental application	CAD/CAM manufactured alumina blasting	SR	Flexural strength decreased by 21-23% from the polished to the alumina blasted sample, and the mechanical characteristics were strongly impacted by SR.
13.	ZrO_2 Block (Kwon *et al.*, 2023)	Dental application	CAD/CAM Milling machined specimen powders	Milling medium and sintering temperature	Mechanical properties increased with sintering temperature and also improved in wet milling medium
14.	3Y-TZP/13-93 BG Bio ceramic composite (Present Work)	Biomedical applications	Air abrasive jet machining (AAJM)	MRR, SR	Unconventional machining approach, MRR 2 to 2.5 times greater at a higher temperature of 600^{o}C, SR was reduced by 36% at 400 ^{o}C, and MRR decreased with bioglass additions